Journal of Cluster Science (2020) 31:117–124
https://doi.org/10.1007/s10876-019-01623-7

ORIGINAL PAPER

Two New NIR Luminescencent Er(III) Coordination Polymers with Potential Application Optical Amplification Devices

Yasemin Acar[1] · Mustafa Burak Coban[1,2] · Elif Gungor[1] · Hulya Kara[3]

Received: 23 May 2019 / Published online: 5 July 2019

Abstract

Two new Er(III)-cluster-based coordination compounds have been synthesized by hydrothermal technique using monosodium 2-sulfoterephthalate (2-stp) and 4,4′-bipyridyl (4,4′-bpy) ligands. Depending on synthetic procedure, monomeric and polymeric Er(III) products, isolated as $\{[Er(2\text{-stp})_2(H_2O)_6]0.2(4,4'\text{-bipy})0.4(H_2O)\}$, **1** and $\{[Er(2\text{-stp})(4,4'\text{-bipy})(H_2O)](H_2O)\}_n$, **2**. Both compounds have been characterized by elemental analysis, FT-IR, UV–visible and single-crystal X-ray diffraction and solid-state photoluminescence. The X-ray structure analyses show that Er atom is surrounded by two 2-stp ligands which have monodentate connection mode forming a monomeric structure in compound **1**. However, in compound **2**, Er atoms are coordinated by four bridging 2-stp ligands which adopt a hexadentate connection mode to form a central symmetrically dimeric building unit. The photoluminescence spectrums of the compounds have been exhibited intense blue emission for **1** and cyan-blue emission for **2**. The band observed in NIR region at 1532 nm (for **1**) and 1540 nm (for **2**) are the typical Er^{III} emission. The excellent NIR luminescent properties, indicating their promising potential applications as gain medium materials in optical amplification devices.

Keywords Er(III) cluster · X-ray structure · Photoluminescence

Introduction

In recent years, the design, synthesis and examining the interesting properties of new materials based on lanthanides coordination compounds have become increasingly relevant area because of their potential applications, for instance, gas storage, separation, catalysis, magnetism, and photoluminescence [1–10]. In lanthanide-based organic frameworks, one of the important subjects is the selection of suitable organic ligands to obtain sensitizing luminescence emission by energy transferring from organic ligands to the central metal ions through antenna effect since the direct excitation of lanthanide ions is nearly impossible. Therefore, in this study, both monosodium 2-sulfoterephthalate (2-stp) as oxygen-based ligand and 4,4′-bipyridyl (4,4′-bpy) as nitrogen based ligand have been especially selected to sensitize the lanthanide luminescence [11–17].

In recent years, the interest towards the compounds containing especially Er(III), Pr(III) and Nd(III) ions among the Ln^{3+}-cluster-based multidimensional coordination compounds, which emit in the near-infrared (NIR) region, has quite increased [18–22]. The studies on the investigation of Er(III) compounds are noteworthy due to their potential applications as an optical signal amplifier in a telecommunication network, and as luminescent probes in biological and medical systems [22–27]. In this work, in the view of the importance of interesting structural and luminescence properties of lanthanide-based coordination compounds, two Er^{+3}-cluster-based coordination

Electronic supplementary material The online version of this article (https://doi.org/10.1007/s10876-019-01623-7) contains supplementary material, which is available to authorized users.

✉ Yasemin Acar
yaseminyahsi@gmail.com

✉ Hulya Kara
hulyasubasat@mu.edu.tr

[1] Department of Physics, Faculty of Science and Art, Balikesir University, Balıkesir, Turkey

[2] Center of Science and Technology Application and Research, Balikesir University, Balıkesir, Turkey

[3] Department of Energy, Graduate School of Natural and Applied Sciences, Mugla Sıtkı Kocman University, Mugla, Turkey

compounds (**1**–**2**) have been synthesized under hydrothermal conditions with using 2-sulfoterephthalate and 4,4′-bipyridyl ligands. Both Er(III) compounds have been determined structurally by single crystal X-ray diffraction method and characterized by UV–Vis, FT-IR and photoluminescence spectroscopy.

Experimental

Materials and Physical Measurements

All solvents and chemicals have been purchased from commercial sources and used without further purification. LECO CHNS-932 analyzer has been used for elemental (C, H, N) analyses. For the PXRD studies, Bruker-AXS D8-Advance system with CuK_α radiation (λ = 1.5418 Å) has been used and also the comparison between experimental and calculated (from CIF's) PXRD patterns was carried out with Mercury 3.8 software. The FT-IR analyses have been performed with a Perkin-Elmer Spectrum 65 instrument in the range of 4000–600 cm^{-1} for both compounds. Solid state UV–visible spectra have been measured at room temperature with an Ocean Optics Maya 2000Pro Spectrophotometer. Room temperature solid-state photoluminescence spectra in the visible and NIR regions have been measured by an ANDOR SR500i-BL Photoluminescence Spectrometer using with the excitation source (349 nm) of a Spectra physics Nd:YLF laser with a 5 ns pulse width and 1.3 mJ of energy per pulse as the source.

An Oxford Xcalibur diffractometer with MoK_α radiation was used for collecting the X-ray intensity data of **1** and **2** at room temperature. Both structures were solved by direct methods using SHELXS [28] and refined by full-matrix least-squares based on $|F_{obs}|^2$ using SHELXL [28] with using Olex2 [29] software. The details of the supramolecular π-interactions were investigated using PLATON 1.17 [30] software. The crystal data and structure refinement details for compounds **1** and **2** are listed in Table 1.

Synthesis of 1

A mixture of $ErCl_3{\cdot}6(H_2O)$ (0.1 mmol), monosodium 2-sulfoterephthalate (2-NaH_2stp; 0.1 mmol) and 4,4′-bipyridyl (4,4′-bpy; 0.1 mmol) in 20 ml of distilled water was sealed into a Parr acid digestion bombs with a Teflon liner (45 mL). The final pH value of this reaction media is close to 4.0. The resultant mixture was heated at 120 °C for 5 days and then slowly cooled to the room temperature. The suitable single crystals of **1** for X-ray diffraction analyses were collected by filtration, washed with distilled water and dried in air. Anal. Calc. $C_{56}H_{66}ErN_8O_{28}S_2$ (Yield 57%): Calcd. C, 43.95; H, 4.35; N, 7.32%; Found: C, 44.17; H, 4.42; N, 7.15%.

Synthesis of 2

A mixture of an equimolar quantity of $ErNO_3{\cdot}5(H_2O)$, 2-NaH_2stp and 4,4′-bpy in 20 ml of distilled water was stirred for 1 h at room temperature and sealed into a bomb equipped with a Teflon liner (45 mL). The pH of the

Table 1 Crystal data and structure refinement for **1** and **2**

	1	**2**
Chemical Formula	$C_{16}H_{18}ErO_{20}S_2{\cdot}8(H_2O){\cdot}4(C_{10}H_8N_2)$	$C_{18}H_{13}ErN_2O_8S{\cdot}(H_2O)$
Formula weight (g mol^{-1})	1530.54	602.64
Crystal system	Monoclinic	Monoclinic
Space group	P2/c	$P2_1/n$
Unit cell dimensions	a = 18.4851 (6) Å	a = 10.8433 (3) Å
	b = 10.7272 (4) Å	b = 16.0521 (5) Å
	c = 19.8043 (8) Å	c = 11.4957 (3) Å
	β = 110.088 (4)°	β = 101.704 (2)°
V ($Å^3$)	3688.2 (3)	1959.31 (10)
Z	2	4
ρ_{calc} (g cm^{-3})	1.378	2.043
μ (mm^{-1})	1.27	4.45
Temperature (K)	292	292
Reflections collected	12,652	7049
Independent reflections	7492 [R_{int} = 0.028]	3968 [R_{int} = 0.024]
Goodness-of-fit on F^2	1.04	1.06
R_1 [$I > 2\sigma(I)$]	R_1 = 0.037	R_1 = 0.029
wR_2 [all data]	wR_2 = 0.083	wR_2 = 0.068

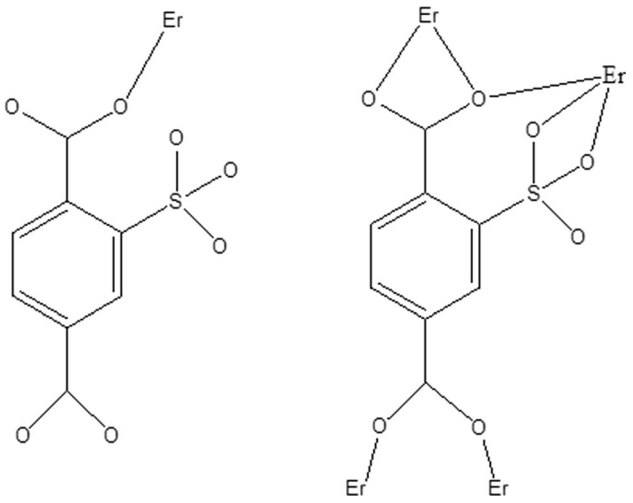

Scheme 1 The coordination mode ($\mu - \eta^1$) in **1** and ($\eta^1{:}\eta^2{:}\eta^1{:}\eta^1{:}$-$\eta^1{:}\eta^1{:}\mu^4$) in **2** of the 2-stp ligand

mixture solution was set to 5–6 by adding NaOH solution (1 mol L^{-1}). The resultant mixture was heated at 140 °C for 5 days and then slowly cooled to the room temperature. The suitable single crystals of **2** for X-ray diffraction analyses were collected by filtration, washed with distilled water and dried in air. Anal. Calc. $C_{18}H_{15}ErN_2O_9S$ (Yield 64%): Calcd. C, 35.86; H, 2.51; N, 4.65%; Found: C, 35.97; H, 2.29; N, 4.85% (Scheme 1).

Result and Discussion

Crystal Structure Determination of 1 and 2

The single crystal X-ray diffraction analyses show that Er(III) complexes have been crystallized in the monoclinic space group $P2/c$ for **1** and $P2_1/n$ for **2**. The molecular structures of compound **1** and **2** with atom labeling have been shown in Figs. 1 and 2, respectively. Although the same donor ligands are used in both complexes, the most important feature that separates the two structures from each other is that complex **1** is monomeric structure while complex **2** is 2D polymeric structure. Two 4,4′-bpy ligand are uncoordinated to Er(III) atom in monomeric compound **1,** while both 4-bpy and 2-stp ligands coordinated to Er(III) atom to give a 2D metal–organic framework in compound **2**. However, the 2-stp ligand is incorporated into the structure as a monodentate mode in **1** while hexadentate mode in **2**. The Er(III) atom is eight coordinated for **1** in a distorted square-antiprism geometry and nine coordinated for **2** as a distorted monocapped square-antiprism geometry. For compound **1**, the environment of Er(III) atom is surrounded by six oxygen atoms from coordinated water molecules and two oxygen atoms each from carboxyl groups of two 2-stp ligands. Er(III) atoms have been bridged by carboxyl oxygen atoms of four 2-stp ligands to give the dimeric units of compound **2**. And these dimeric moieties have been connected via both carboxyl and sulfo oxygen atoms of 2-stp ligands to give the 2D framework structure of **2**. The distances between Er(III) atom and

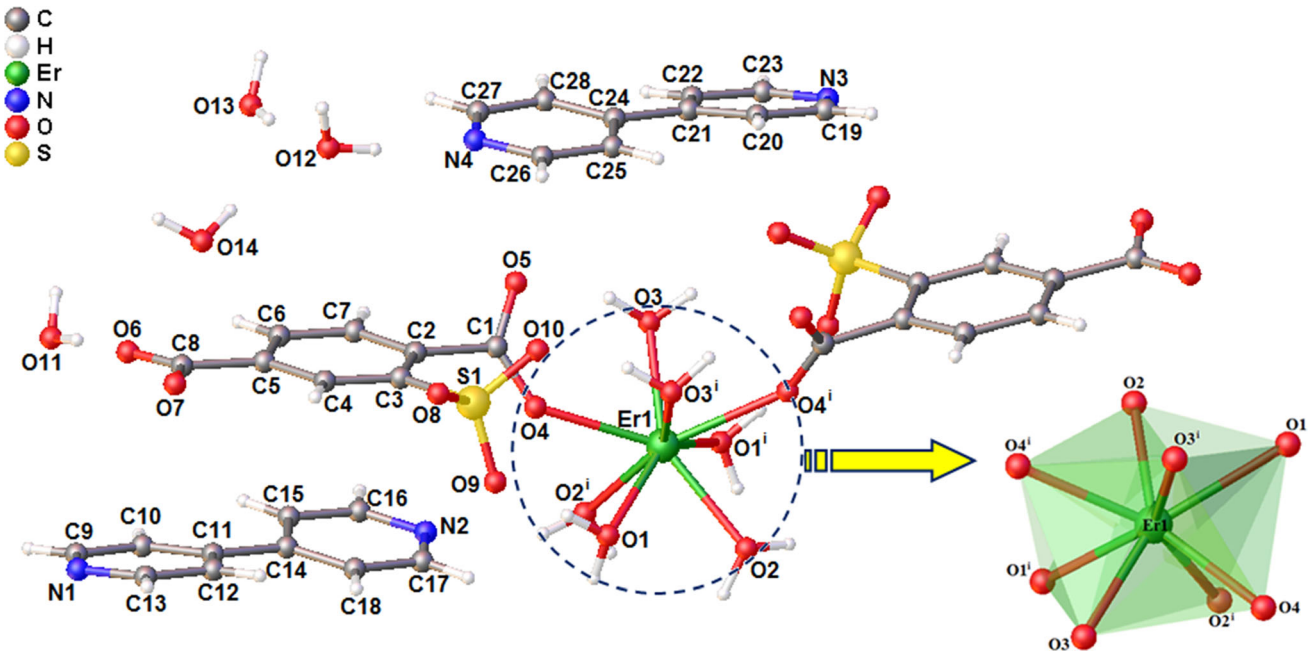

Fig. 1 View of the molecular structure of **1** and the coordination environment of Er^{III} atom (Symmetry code: i = 1 − x, y, 3/2 − z)

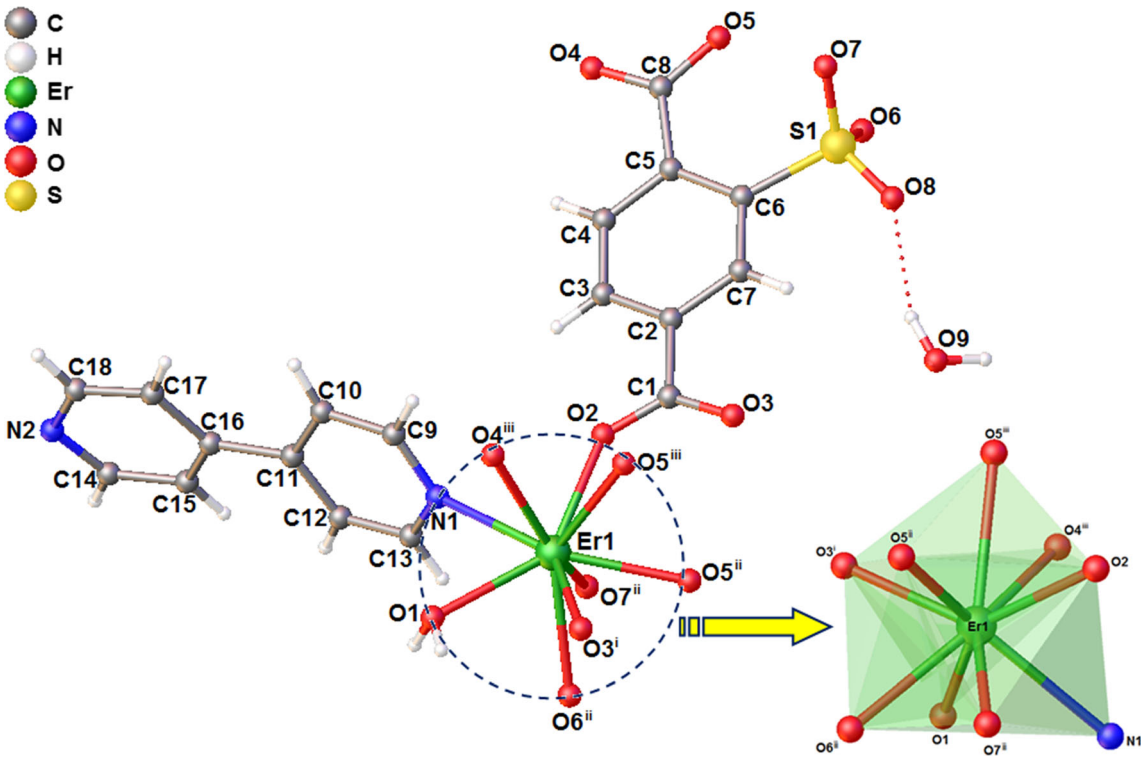

Fig. 2 View of the molecular structure of **2** and the coordination environment of Er^{III} atom [Symmetry code: (1) $-x+1, -y+1, -z+2$; (2) $-x+1/2, y+1/2, -z+3/2$; (3) $x+1/2, -y+1/2, z+1/2$]

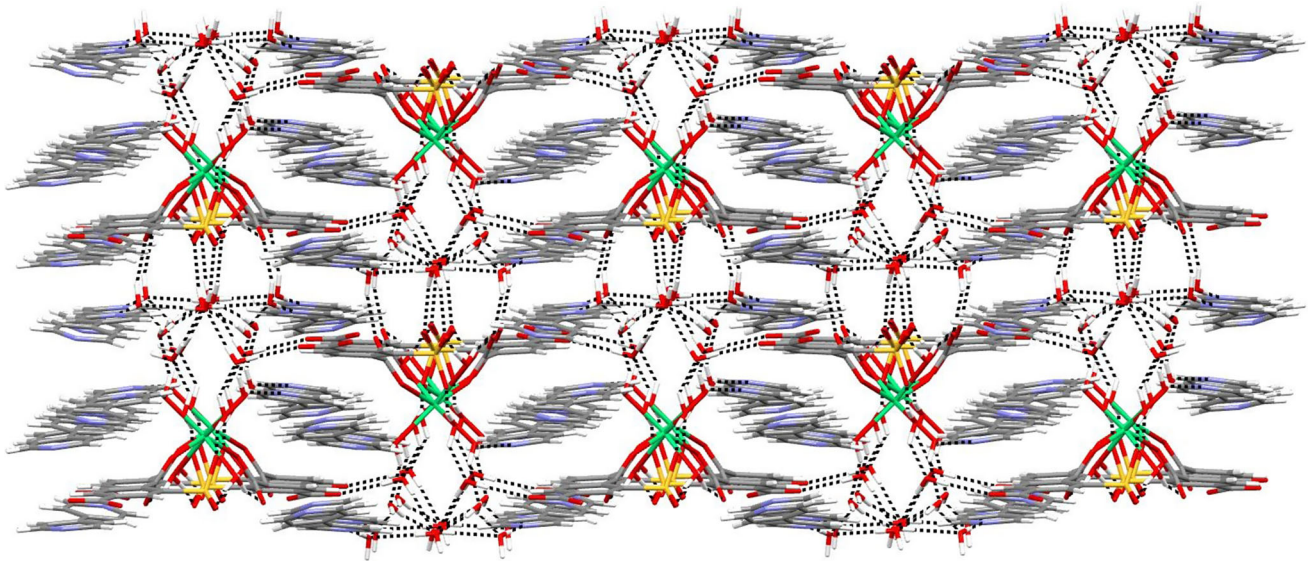

Fig. 3 3D hydrogen-bonded network of compound **1**

oxygen atoms from coordinated water molecules are in the range of 2.310(2)–2.413(2) Å for both compound and also the average bond distances between Er(III) and carboxyl oxygens are 2.358 Å for **1** and 2.375 Å for **2**. All bond distance and angles are listed in Table S1 for **1** and in Table S2 for **2** and also comparable to similar structures [22, 31–34]. Hydrogen bond geometries and the distances between ring centroids have been listed in Table S3 and Table S4 for compound **1** and **2**, respectively. As seen in Figs. 3 and 4, both Er(III) compounds are formed in 3D networks via strong hydrogen bonds.

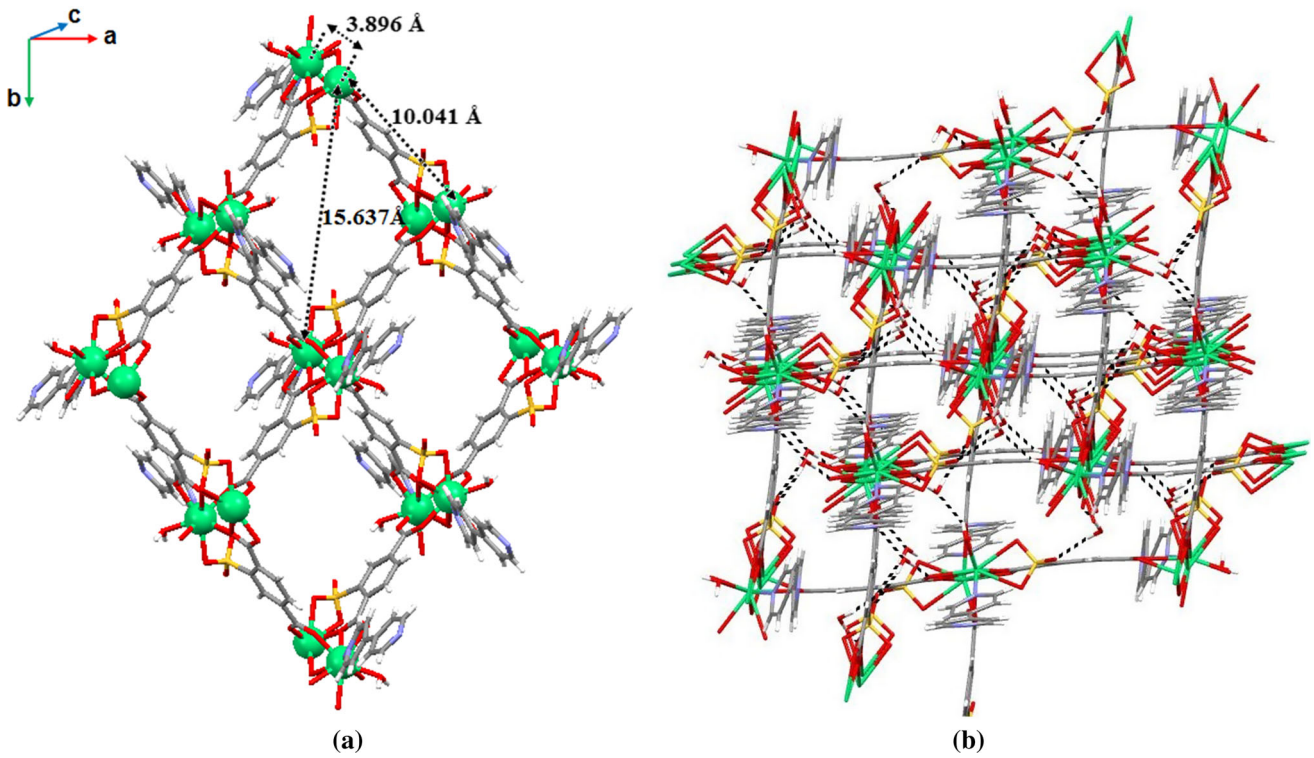

Fig. 4 **a** A view of the 2D structure of compound **2** (A lattice water molecule is omitted for clarity) **b** 3D hydrogen-bonded network of compound **2**

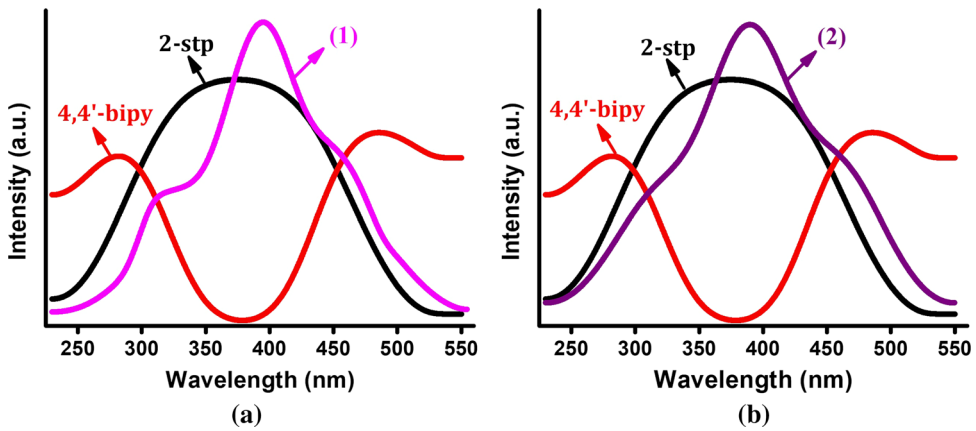

Fig. 5 The absorption spectrum of **a** compounds **1** and **b** **2** with the free ligands (2-stp and 4,4′-bipy)

FT-IR Spectra

The IR spectra of free ligands and Er(III) compounds (**1** and **2**) have been investigated in the solid state in the range of 4000–600 cm^{-1} (see Fig. S1). Comparing the IR spectra of the free 2-stp ligand with those of complexes **1**–**2**, the characteristic vibration peaks of both COOH and SO_3H around 1740–1692 cm^{-1} were absent, indicating these protons were deprotonated [9, 15, 35]. The broad band at about 3300 cm^{-1} for both compounds shows the presence of ν(O–H) stretching frequency associated with coordinated water molecules [34, 36]. In the spectra of **1** and **2**, ν_{as}(COO) and ν_s(COO) were observed at about 1570 and 1410 cm^{-1} for both complexes, respectively [15, 37].

Solid State UV–Vis Spectra

The UV–Vis absorption spectra of both Er(III) compounds have been investigated in solid state and shown in Fig. 5 within the comparison of their free ligands 2-stp and 4,4′-

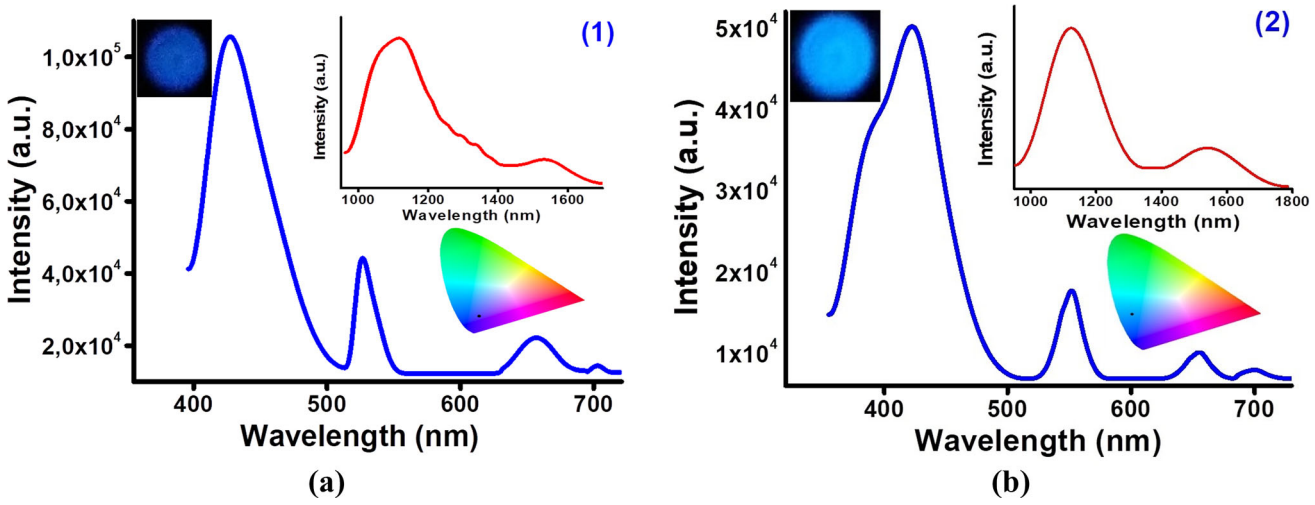

Fig. 6 The solid-state photoluminescence spectrum of **a** compound **1** and **b** compound **2** (upper-right inset: the corresponding emission spectrum in the NIR region for compounds **1** and **2**). The upper-left images are the luminescent images of the compounds and bottom-right images are their CIE color chromaticity diagrams

bipy. There have been two absorption bands at 282 and 485 nm for 4,4′-bipy ligand while there have been one maxima at 375 nm for 2-stp ligand. The compounds have absorption bands at 395 nm for **1** and 390 nm for **2** in the near UV–Vis region below 400 nm, which is a dominant feature in the absorption spectrum. These near UV absorptions may be attributed π–π* or n–π* transition of the free ligands [13, 38–40]. The bands have been slightly shifted towards lower energy which signifies the lanthanide ion coordination with 2-stp ligand [41, 42].

Photoluminescence Properties

In the visible and NIR regions, the photoluminescent properties of the free ligands and compounds **1** and **2** upon excitation at λ_{ex} = 349 nm were investigated in the solid state at room temperature (Fig. 6). The four emission bands in the UV–visible region appear at λ_{max} = 427, 526, 657, 702 nm for compound **1** and λ_{max} = 422, 551, 655, 700 nm for compound **2** which are assigned to the *f*–*f* transition $^4F_{5/2} \rightarrow {}^4I_{15/2}$, $^2H_{11/2} \rightarrow {}^4I_{15/2}$, $^4F_{9/2} \rightarrow {}^4I_{15/2}$ and $^4F_{7/2} \rightarrow {}^4I_{13/2}$, respectively [22, 34, 43]. The coordinates of CIE colors which are found to be (0.21; 0.14) for **1** and (0.12; 0.26) for **2**, respectively, have been calculated from the emission spectra data. As seen in their CIE chromaticity diagram which has been shown in Fig. 6, it is found that the CIE coordinates are located in the blue region for **1** and in the cyan-blue region for **2**, respectively.

In the NIR region, two emission bands appear at λ_{max} = 1116, 1532 nm for **1** and λ_{max} = 1123, 1540 nm for **2** consisting of the $^4I_{11/2} \rightarrow {}^4I_{15/2}$ and $^4I_{13/2} \rightarrow {}^4I_{15/2}$ transitions of Er^{3+}, respectively [34, 44–47]. The bands observed at 1532 nm (for **1**) and 1540 nm (for **2**) are the typical Er^{III} emission which corresponds to that the wavelength of the low-loss transmission window in telecommunication fibers and this transition is currently employed in the telecommunication area [48–50]. Moreover, their FWHM values are 73 nm for **1** and 149 nm for **2**, respectively, which are of significance for optical amplification [51–53].

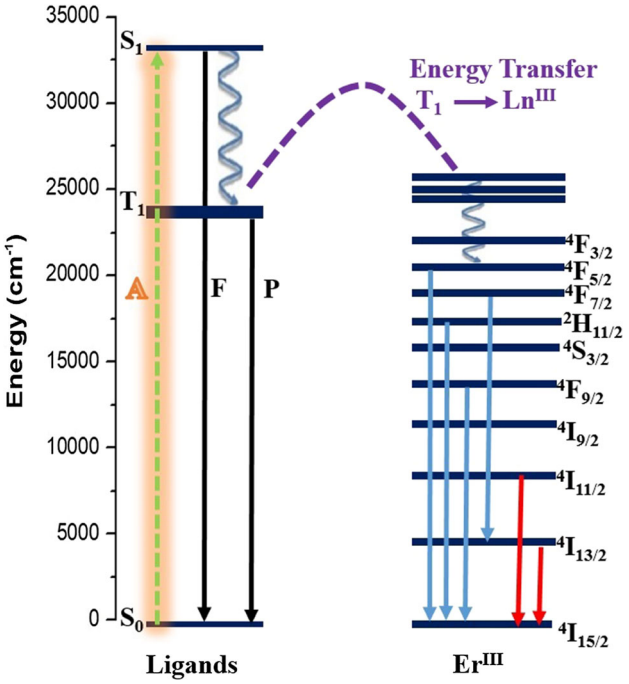

Fig. 7 Scheme of the energy transfer mechanism and PL processes

The energy transfer process which is called as "antenna effect" or "luminescence sensitization" occurs by the ligand–metal energy transfer as the excitation of lanthanide

ions in a direct way is nearly impossible [50, 54]. The schematic energy levels and the energy transfer processes for Er(III) compounds are shown in Fig. 7 to further understand the sensitization mechanism of the erbium ion by organic ligands. The excitation of the 2-stp and 4,4′-bpy ligands at λ = 349 nm led to Visible/NIR luminescence, associated with the transitions of trivalent erbium ion. The ground state absorption $S_0 \rightarrow S_1$ in the ligand moiety occurs under this direct excitation and the energy of the lowest excited singlet level is transferred to the T_1 triplet level via intersystem crossing (ISC). And the whole energy-transfer process is completed with the subsequent energy transfer from triplet level to the energy levels of Er^{3+} ion in which resulting in the characteristic emissions of the sensitized trivalent lanthanide ion.

Conclusion

In this work, two erbium based coordination compounds, (**1**–**2**) have been synthesized by the use of 2-sulfotereph-thalate as oxygen donor ligand and 4,4′-bipyridyl as nitrogen donor ligand under hydrothermal conditions. These Er(III) compounds have been characterized by single crystal X-ray diffraction analysis, UV–Vis, FT-IR, and photoluminescence spectroscopy. X-ray structural analysis of both compounds shows that the coordination geometry around the eight coordinated Er(III) ions for **1** and nine coordinated Er(III) ions for **2** can be described as a distorted square-antiprism and a distorted monocapped square-antiprism, respectively. However, 2-stp ligand bridged in two different modes, making a significant difference in the structure of compound **1** and **2**. The 2-stp ligand coordinated in monodentate mode and free 4-bpy ligand in compound **1**, make the structure monomer while 2-stp ligand coordinated in hexadentate mode and bridged 4-bpy ligands in compound **2**, make the structure organic framework. The dimeric Er(III) units form square-like frame structures in the 2D network, and thus they form the 3D network structure with strong hydrogen bonds in compound **2**. The photoluminescence properties of **1** and **2** have been investigated in the solid state at the room temperature. In the visible regions, intense blue emission for compound **1** and cyan-blue emission for compound **2** have been exhibited under the excitation of UV light at λ_{ex} = 349 nm.

Supplementary Material

The crystallographic data in detail for both compounds have been deposited with the CCDC (Cambridge Crystallographic Data Centre) No 1905604 (for **1**) and CCDC No 1905605 (for **2**). These data on request can be obtained free of charge via http://www.ccdc.cam.ac.uk (or e-mail: deposit@ccdc.cam.ac.uk).

Acknowledgements The authors thanks to the Research Funds of Balikesir University (Grant No. BAP-2017/183) for the financial support, Dr. Muhittin Aygun and Dokuz Eylül University (Grant No. 2010.KB.FEN.13) for the use of the Agilent Xcalibur Eos diffractometer and also to BUBTAM (Balikesir University Science and Technology Application and Research Center) for the use of the Photoluminescence Spectrometer.

References

1. B. Chen, C. Liang, J. Yang, D. S. Contreras, Y. L. Clancy, E. B. Lobkovsky, O. M. Yaghi, and S. Dai (2006). *Angew. Chem. Int. Ed.* **45**, 1390.
2. C. Biswas, P. Mukherjee, M. G. B. Drew, C. J. Gómez-García, J. M. Clemente-Juan, and A. Ghosh (2007). *Inorg. Chem.* **46**, 10771.
3. J. J. I. Perry, J. A. Perman, and M. J. Zaworotko (2009). *ChemInform* **40**, 1400.
4. D. Zhao, D. Yuan, and H.-C. Zhou (2008). *Energy Environ. Sci.* **1**, 222.
5. M. H. Alkordi, Y. Liu, R. W. Larsen, J. F. Eubank, and M. Eddaoudi (2008). *J. Am. Chem. Soc.* **130**, 12639.
6. W. Zhang, H. Y. Ye, and R. G. Xiong (2009). *Coord. Chem. Rev.* **253**, 2980.
7. D. Shi, Y. Ren, H. Jiang, B. Cai, and J. Lu (2012). *Inorg. Chem.* **51**, 6498.
8. R. Decadt, K. Van Hecke, D. Depla, K. Leus, D. Weinberger, I. Van Driessche, P. Van Der Voort, and R. Van Deun (2012). *Inorg. Chem.* **51**, 11623.
9. G. Oylumluoglu, M. B. Coban, C. Kocak, M. Aygun, and H. Kara (2017). *J. Mol. Struct.* **1146**, 356.
10. G. Oylumluoglu (2018). *J. Clust. Sci.* **29**, 649.
11. Y. X. Ren, M. An, H. M. Chai, M. L. Zhang, and J. J. Wang (2015). *Zeitschrift Fur Anorg. Und Allg. Chemie* **641**, 525.
12. M. B. Coban, U. Erkarslan, G. Oylumluoglu, M. Aygun, and H. Kara (2016). *Inorganica Chim. Acta* **447**, 87.
13. M. B. Coban, C. Kocak, H. Kara, M. Aygun, and A. Amjad (2017). *Mol. Cryst. Liq. Cryst.* **648**, 202.
14. M. B. Coban, A. Amjad, M. Aygun, and H. Kara (2017). *Inorganica Chim. Acta* **455**, 25.
15. M. B. Coban (2018). *J. Mol. Struct.* **1162**, 109.
16. S. Chooset, A. Kantacha, K. Chainok, and S. Wongnawa (2018). *Inorganica Chim. Acta* **471**, 493.
17. D. H. Kim, H. S. Kim, C. H. Kwak, J. H. Lee, S. C. Jung, H. G. Ahn, and M. C. Chung (2010). *J. Nanosci. Nanotechnol.* **10**, 3420.
18. J. P. Leonard and T. Gunnlaugsson (2005). *J. Fluoresc.* **15**, 585.
19. J. C. G. Bünzli (2006). *Acc. Chem. Res.* **39**, 53.
20. M. A. Katkova, A. P. Pushkarev, T. V. Balashova, A. N. Konev, G. K. Fukin, S. Y. Ketkov, and M. N. Bochkarev (2011). *J. Mater. Chem.* **21**, 16611.
21. L. F. Marques, H. P. Santos, C. C. Correa, J. A. L. C. Resende, R. R. da Silva, S. J. L. Ribeiro, and F. C. Machado (2016). *Inorganica Chim. Acta* **451**, 41.
22. P. Martín-Ramos, M. D. Miranda, M. R. Silva, M. E. S. Eusebio, V. Lavín, and J. Martín-Gil (2013). *Polyhedron* **65**, 187.
23. P. Martín-Ramos, M. R. Silva, C. Coya, C. Zaldo, Á. L. Álvarez, S. Álvarez-García, A. M. Matos Beja, and J. Martín-Gil (2013). *J. Mater. Chem. C* **1**, 2725.

24. P. Martín-Ramos, C. Coya, Á. L. Álvarez, M. Ramos Silva, C. Zaldo, J. A. Paixão, P. Chamorro-Posada, and J. Martín-Gil (2013). *J. Phys. Chem. C* **117**, 10020.
25. S. V. Eliseeva and J. C. G. Bünzli (2011). *New J. Chem.* **35**, 1165.
26. A. Mech, A. Monguzzi, F. Meinardi, J. Mezyk, G. Macchi, and R. Tubino (2010). *J. Am. Chem. Soc.* **132**, 4574.
27. S. Penna, A. Reale, R. Pizzoferrato, G. M. Tosi Beleffi, D. Musella, and W. P. Gillin (2007). *Appl. Phys. Lett.* **91**, 021106.
28. G. M. Sheldrick (2015). Acta Crystallogr. Sect. C. *Struct. Chem.* **71**, 3.
29. O. V. Dolomanov, L. J. Bourhis, R. J. Gildea, J. A. K. Howard, and H. Puschmann (2009). *J. Appl. Crystallogr.* **42**, 339.
30. A. L. Spek (2009). *Acta Crystallogr. Sect. D Biol. Crystallogr.* **65**, 148.
31. Q. Zhong, H. Wang, G. Qian, Z. Wang, J. Zhang, J. Qiu, and M. Wang (2006). *Inorg. Chem.* **45**, 4537.
32. P. Martín-Ramos, P. S. P. Silva, P. Chamorro-Posada, M. R. Silva, B. F. Milne, F. Nogueira, and J. Martín-Gil (2015). *J. Lumin.* **162**, 41.
33. Z. Ahmed, R. E. Aderne, J. Kai, J. A. L. C. Resende, H. I. Padilla-Chavarría, and M. Cremona (2017). *RSC Adv.* **7**, 18239.
34. U. Erkarslan, A. Donmez, H. Kara, M. Aygun, and M. B. Coban (2018). *J. Clust. Sci.* **29**, 1177.
35. Z. Wang, S. Zheng, Z. Markus, M. Kou-Lin, H.-J. You, and X.-Z. Yu (2002). *Inorg. Chem. Commun.* **5**, 230.
36. Z. Lu, L. Wen, J. Yao, H. Zhu, and Q. Meng (2006). *CrystEngComm* **8**, 847.
37. S. Bibi, M. Sharifah, N. S. Abdul Manan, T. Huma, B. M. Yamin, and S. N. Abdul Halim (2018). *Transit. Met. Chem.* **43**, 53.
38. J. L. Chen, Y. S. Luo, G. P. Gao, J. L. Zhao, L. Qiu, N. Liu, L. H. He, S. J. Liu, and H. R. Wen (2016). *Polyhedron* **117**, 388.
39. Y. Acar, H. Kara, E. Gungor, and M. B. Coban (2018). *Mol. Cryst. Liq. Cryst.* **664**, 165.
40. L. Vittaya, N. Leesakul, S. Saithong, S. Phongpaichit, P. Chumponanomakun, T. Boonprab, K. Chainok, and Y. Tantirungrotechai (2017). *Sci. Asia* **43**, 175.
41. M. B. Coban (2019). *J. Mol. Struct.* **1177**, 331.
42. S. Bibi, S. Mohamad, N. S. Abdul Manan, J. Ahmad, M. A. Kamboh, S. M. Khor, B. M. Yamin, and S. N. Abdul Halim (2017). *J. Mol. Struct.* **1141**, 31.
43. X. Sun, B. Li, L. Song, J. Gong, and L. Zhang (2010). *J. Lumin.* **130**, 1343.
44. W. Wu, X. Zhang, A. Y. Kornienko, G. A. Kumar, D. Yu, T. J. Emge, R. E. Riman, and J. G. Brennan (2018). *Inorg. Chem.* **57**, 1912.
45. S. Destri, M. Pasini, W. Porzio, F. Rizzo, G. Dellepiane, M. Ottonelli, G. Musso, F. Meinardi, and L. Veltri (2007). *J. Lumin.* **127**, 601.
46. P. Martín-Ramos, P. Chamorro-Posada, M. Ramos Silva, P. S. Pereira Da Silva, I. R. Martín, F. Lahoz, V. Lavín, and J. Martín-Gil (2015). *Opt. Mater. (Amst).* **41**, 139.
47. C. Q. Wan, X. Li, C. Y. Wang, and X. Qiu (2009). *J. Mol. Struct.* **930**, 32.
48. S. Sarkar, V. N. K. B. Adusumalli, V. Mahalingam, and J. A. Capobianco (2015). *Phys. Chem. Chem. Phys.* **17**, 17577.
49. R. Van Deun, P. Nockemann, C. Görller-Walrand, and K. Binnemans (2004). *Chem. Phys. Lett.* **397**, 447.
50. F. Artizzu, M. L. Mercuri, A. Serpe, and P. Deplano (2011). *Coord. Chem. Rev.* **255**, 2514.
51. Q. Sun, P. Yan, W. Niu, W. Chu, X. Yao, G. An, and G. Li (2015). *RSC Adv.* **5**, 65856.
52. D. Liu, C. Li, Y. Xu, D. Zhou, H. Wang, P. Sun, and H. Jiang (2017). *Polymer (Guildf).* **113**, 274.
53. S. G. Roh, N. S. Baek, K. S. Hong, J. B. Oh, and H. K. Kim (2004). *Mol. Cryst. Liq. Cryst.* **425**, 167.
54. J. M. Lehn (1990). *Angew. Chem. Int. Ed. Engl.* **29**, 1304.